Optimisation of representative elementary area (REA) for the preparation of lineament density map of fractured rock aquifer

H Jia* and L Lin

Water Geoscience Unit, Council for Geoscience, Private Bag X112, Pretoria, South Africa

Abstract

The lineament density map derived from remote sensing data of the fractured rock terrain plays an important role in the evaluation of the groundwater resource in the associated fractured aquifer. Application of the lineament density map frequently encounters the problems of whether the density map is representative of an area and whether the map can be effectively applied at a regional scale. Lineament data captured from Landsat ETM+ imagery in 7 domain areas in the Table Mountain Group (TMG) sandstone terrain were used to compute and analyse lineament densities. Methods of determining representative elementary area (REA) on a domain-area scale and on a study-area scale were developed, respectively, based on the power law relationship of lineament densities with computing cell sizes, linear relationship of REAs with domain-area sizes, and the power law relationship of REA percentages with domain-area sizes. Using the function convergence criterion of curve slope less than 1º and measuring dimension in units of area (L^2) other than units of length (L), the REA of each domain area can be accurately determined. REA scale-effect analysis helps to optimise the determination of REA in a study area, and the optimisation of REAs may in turn improve the lineament density map generated for regional groundwater studies.

Keywords: lineament density, representative elementary area (REA), fractured rock aquifer, Table Mountain Group (TMG)

Introduction

Lineament mapping from satellite imagery or aerial photography is an important approach to regional groundwater investigation and exploration. With the increasing availability of high-resolution imagery of the earth, more and more hydrogeologists have been making use of remote sensing techniques for studying hydrogeological conditions (Schowengerdt et al., 1979; Mabee et al., 1994; Kresic, 1995; Drury et al., 2001), site investigation (Sander et al., 1996; 1997), groundwater monitoring (Rodell and Famiglietti, 2002), and groundwater protection and resource evaluation (Koch and Mather, 1997; Bressan and Anjos, 2003). As groundwater is not readily perceptible from remote sensing data, surface indicators have to be used to infer the subsurface condition which controls groundwater occurrence. Lineaments captured from imagery often provide a crucial clue on the interpretation and analysis of groundwater flow regimes. The main assumption that underlies all lineament analyses is that the linear features (O'Leary et al., 1976; Waters et al., 1990), when properly identified, represent the surface manifestations of transmissive fracture framework of low permeability rocks (Degnan et al., 2002). Lineaments are usually characterised by azimuth and length distributions, length density (L_d, total length of lineaments per unit area), frequency (L_f, total numbers of lineaments per unit area), and intersection point density (L_c, total number of lineament intersection points per unit area). Lineament density maps are hence important for the study of groundwater in fractured aquifers, especially when they are incorporated with other pertinent maps via GIS integration.

Many efforts have contributed to the application of lineament densities to aquifer properties (Bracq and Delay, 1997; Edet et al., 1998) and borehole productivity (Gustafsson, 1994; Owen et al., 2003). They all seemed to conclude that lineament densities have relations in different degrees to the occurrence of groundwater in areas with well-exposed bedrocks. However, the results can seldom be practical if density maps are not properly prepared or not representative of a study area. Usually, preparation of a lineament density map is done by segmenting lineaments with squared or circular grid cells. The L_d, L_f, and L_c are computed for each cell, after which the density map can be generated through various interpolation techniques. The theoretical basis of lineament segmenting was discussed in detail by Mostafa and Qari (1995). No matter which type of grid cell is used, the choice of cell size is not arbitrary but obtained through a statistical study of the spatial properties of lineaments (Bracq and Delay, 1997; Casas et al., 2000). The necessity of estimating a best-fitting cell size for lineament densities leads to the application of representative elementary area (REA), which is derived from the concept of the representative elementary volume (Bear, 1972). The concept of REA was coined by Beven et al. (1988) and has been used to analyse spatial heterogeneity and scale-dependent problems by Wood et al. (1988) and Woods et al. (1995) in studies of catchment hydrological response, aiming to determine a minimum area of catchment at which the hydrological response keeps relatively stationary along with the increase of catchment areas.

There has been no consensus over the criterion for the determination of REA under the scale of consideration, and it is mostly based on visual analysis (Tam et al., 2004), depending on the objective of a given study. In this respect, Bygaart and Protz (1999) and Kim et al. (2004), in their studies of pedo-features and lineament densities, respectively, suggest that the size of REA can be determined when a level of value change is not beyond ±10% in 3 successive measurement points. However, a

* To whom all correspondence should be addressed.
☎ +2712 841-1277; fax: +276 649-1555;
e-mail: hjia@geoscience.org.za
Received 15 May 2009; accepted in revised form 30 March 2010.

range of ±10% appears optional because the REA measured can be affected by:

- Number and size step of cells (Bygaart and Protz, 1999)
- Measuring dimensions (e.g. length or area of cells)
- Measured parameters of which the spatial variations are different

As will be discussed later, the method of determining REA, proposed in this paper, adds a new feature to the characterisation of lineaments, which may enhance the current criterion.

In this paper, the relationship between lineament densities (viz. L_d, L_f and L_c) and computing cell size is examined in selected domain areas of Table Mountain Group (TMG) sandstone terrain of South Africa. A method is developed to reveal the relationship between lineament densities and cell sizes, in order to produce an optimal REA estimate for the appropriate application of lineament densities to the quantification of groundwater resources in the TMG areas. In addition, the scale effect of the REAs is analysed, which will help to solve the scale-dependent problems associated with best fitting REA, and may further shed light on understanding of scale-dependent spatial problems in the fields of aquifer property determinations, water resource evaluations, and numerical modelling applications, on the basis of regional study.

Study area

Currently, groundwater development in South Africa is mainly concentrated on fractured rock aquifers, within which there are 3 major aquifer systems: dolomite, the TMG sandstones, and Karoo sediments with dolerite intrusions. The TMG extends from the Western Cape to Eastern Cape in South Africa (Fig. 1a), comprising a thick sequence of hard sedimentary rocks dominated by fractured sandstones with a thickness ranging from 900 m to 5 000 m (Rust, 1973). The TMG covers an area of about 248 400 km^2 with 37 000 km^2 outcrops that constitute high mountain terrains in the Western and Eastern Cape Provinces.

Tectonically, the TMG rocks have been reconstructed by several phases of crustal movements and various types of discontinuities in the form of joints, faults and unconformities have been created. Structures in the TMG were produced by the development of the Cape Fold Belt during the Permo-Triassic Cape Orogeny (De Beer, 2001), extending from Australia through Antarctica and South Africa to South America (McCarthy and Rubidge, 2005). Further tectonic modification of the area occurred during the fragmentation of south-western Gondwanaland during the late Mesozoic, disrupting previous topographies with a series of tensile and dextral displacements. Some of the discontinuities have been reactivated since the post-Karoo tectogenesis which complicated existing fracture systems. These secondary structural voids in the TMG sandstones and siltstones constitute most of the fracture spaces allowing for groundwater storing or moving.

The study area is situated at the southern and western branches of the Cape Fold Belt (Fig. 1a), comprising a series of folds and faults extending NW-SE, NE-SW and near W-E. Due to the lithologies and geomorphologies, many of the TMG outcrops are well exposed as bare rocks but extremely difficult to access. This gives rise to the potential to use remote sensing data to study the hydrogeological conditions on the basis of lineament analysis in the fractured rocks. As lineament analysis requires the location and distribution of lineaments to be closely representative of fracture-correlated featurese, the domain areas chosen should display very good rock exposures on images. Thus areas with too many or too large barren lineament windows have to be excluded. This may reduce the selection of available study areas, but increases the quality and consistency of lineament data interpreted. For this study, 7 domain areas in the south-western TMG outcrops, labelled as A1~A7, with the size ranging from 6.25 km^2 to 225 km^2 (Fig. 1b), were selected from a number of candidate areas for lineament and density map analyses.

Lineament analysis and density map

The Landsat 7 EMT$^+$ imagery was applied for on-screen data capturing by comparison of the spatial resolutions of various sources of satellite imagery and aerial photography covering the TMG area. To minimise the uncertainty associated with lineament identification, existing geological and geomorphologic information was used in conjunction with interpretive knowledge. Lineament length and orientation, lineament length density, frequency and intersection point density were then computed using Visual Basic for Application (VBA) scripts developed in ArcMap, and density maps were also generated in ArcGIS using ordinary kriging.

Lineament mapping and analysis

Meaningful interpretation of lineaments associated with the structural framework is largely dependent on the quality of imagery, acquaintance with the area's background, and the approach to acquiring lineament data. In this study lineament mapping was done by using Landsat 7 ETM$^+$ imagery (UTM zones: S-34-30) that covers the western half of the TMG area. The existing lithostratigraphic, geomorphologic, and structural information was also used to provide reference points during the mapping. The imagery comprises 7 multi-spectral bands and 1 panchromatic band. It had already been linearly enhanced and projected before being imported to GIS. In comparison with conventional aerial photography (1/50 000), the imagery has better spatial resolution which allows tracing of lineaments with 65 m minimum length (approximately twice its spatial resolution). To enhance the confidence of lineament interpretation, multiple interpreters were employed to trace as many visible lineaments reflected on the imagery as possible. The data from various interpreters were carefully compared at the same scale and then combined to one shape file. In the meantime, each of the lineaments was identified, in order to avoid the non-fracture-correlated lineaments as much as possible. The major problem encountered during the lineament tracing with the images was the sun azimuth effect (Woodford and Chevallier, 2002) which created a bias toward north-eastern striking lineaments; therefore patience was required to identify such linear features. After the mapping of a domain area was done, each lineament length and orientation was computed for the distribution and density analyses. The mapping and statistical results of the lineaments in the 7 domain areas are presented in Fig. 1b.

The distribution patterns of lineament lengths and orientations are very useful for the study of fractured-rock aquifers (Kulatilake and Panda, 2000), especially in the case where the measurement of fracture lengths and orientations on the surface is unable to yield sufficient data. A quantitative analysis was carried out to determine the distribution of lineament orientations and lengths in each domain area. The results of directional analysis showed that there are principally 3 striking

Available on website http://www.wrc.org.za
ISSN 0378-4738 (Print) = Water SA Vol. 36 No. 3 April 2010
ISSN 1816-7950 (On-line) = Water SA Vol. 36 No. 3 April 2010

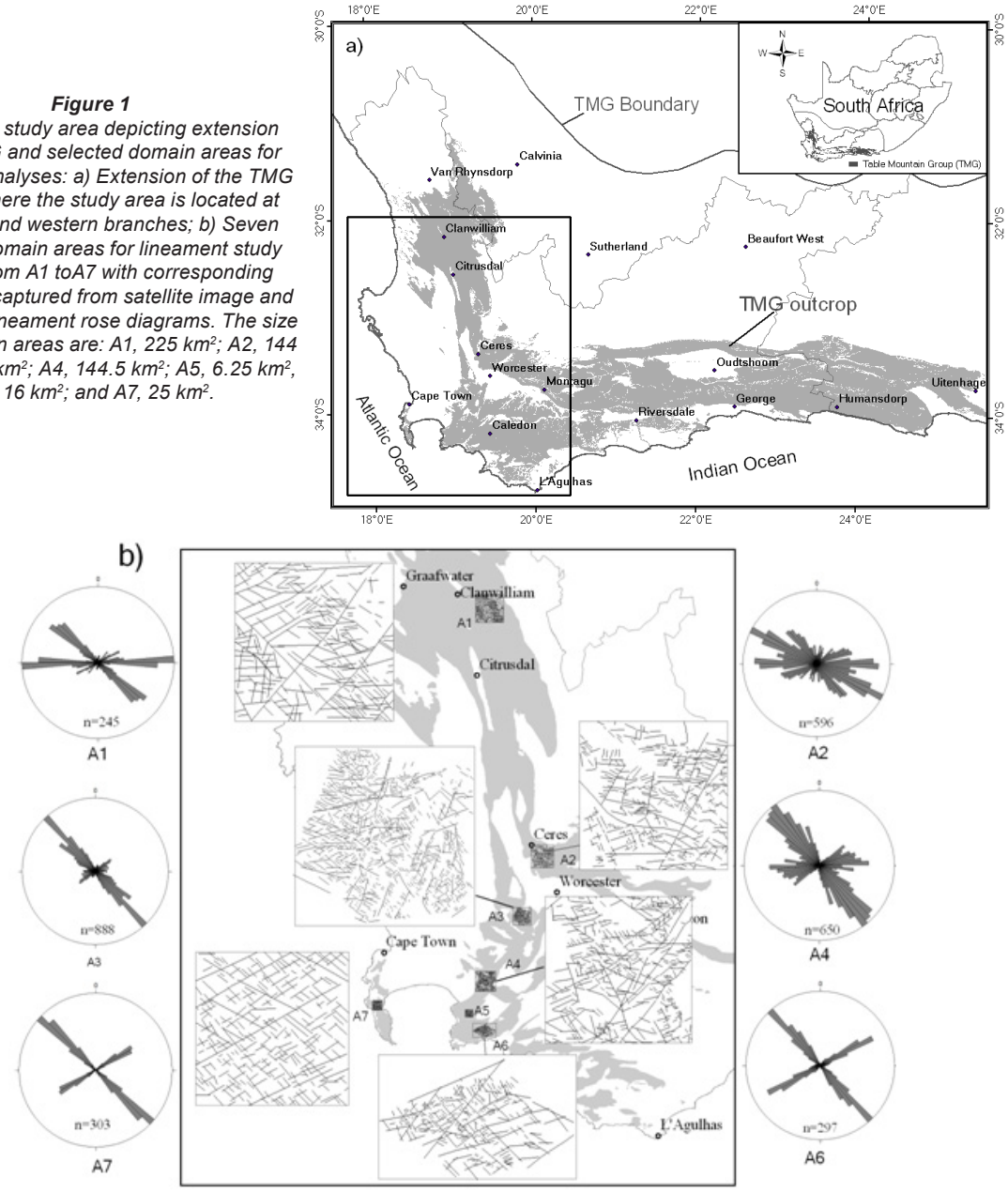

Figure 1

Map of the study area depicting extension of the TMG and selected domain areas for lineament analyses: a) Extension of the TMG outcrop where the study area is located at southern and western branches; b) Seven selected domain areas for lineament study labeled from A1 toA7 with corresponding lineaments captured from satellite image and associated lineament rose diagrams. The size of the domain areas are: A1, 225 km^2; A2, 144 km^2; A3, 45 km^2; A4, 144.5 km^2; A5, 6.25 km^2, A6, 16 km^2; and A7, 25 km^2.

directions: NE-SW, NW-SE, and near E-W in the 7 domain areas (Fig. 1b). According to the distribution of the orientations, these areas can be grouped into 4 categories probably representing different fracture patterns and tectonic stress conditions from the north to the south of the study area:

- A1 in the northwest
- A2 in the core of structural syntax zone
- A3 and A4 in the middle south
- A5, A6 and A7 in the southernmost areas where the lineaments are merely striking to NE-SW and NW-SE

The recorded lineament length ranges from 60 m to 17 450 m with mean values ranging from 351 m to 1 984 m in the 7 domain areas. No significant differences in the distribution of lineament length can be found from the number-length histograms (Fig. 2). They all appear to have a lognormal distribution with various mean values and standard deviations. This distribution pattern is thought to prevail in the TMG sandstone terrain, regardless of the size of a domain area.

Generation of lineament density maps

Based on lineament data obtained and identified from satellite imagery, preparation of lineament density maps, first of all, requires a careful design of mesh grids (rectangular or circular cells) which are used to crop the information of coordinates, lineament segment numbers and lengths, and densities. In this study, we used squared grids, instead of rectangular and circular grids, for the generation of density maps.

The 1st step of the density map processing is to generate an equally-spaced squared grid, which is automatically divided from a mesh framework controlled by total numbers of rows/columns (viz. i, j) and associated power numbers (2^i) (Fig. 3), depending on the size of a cell under consideration. For the purpose of computation and positioning of lineament density values, the area and central coordinates of each cell have to be calculated using the table field calculator after the grid division. The 2nd step is to crop lineament segments completely within each cell in terms of total length, gross number,

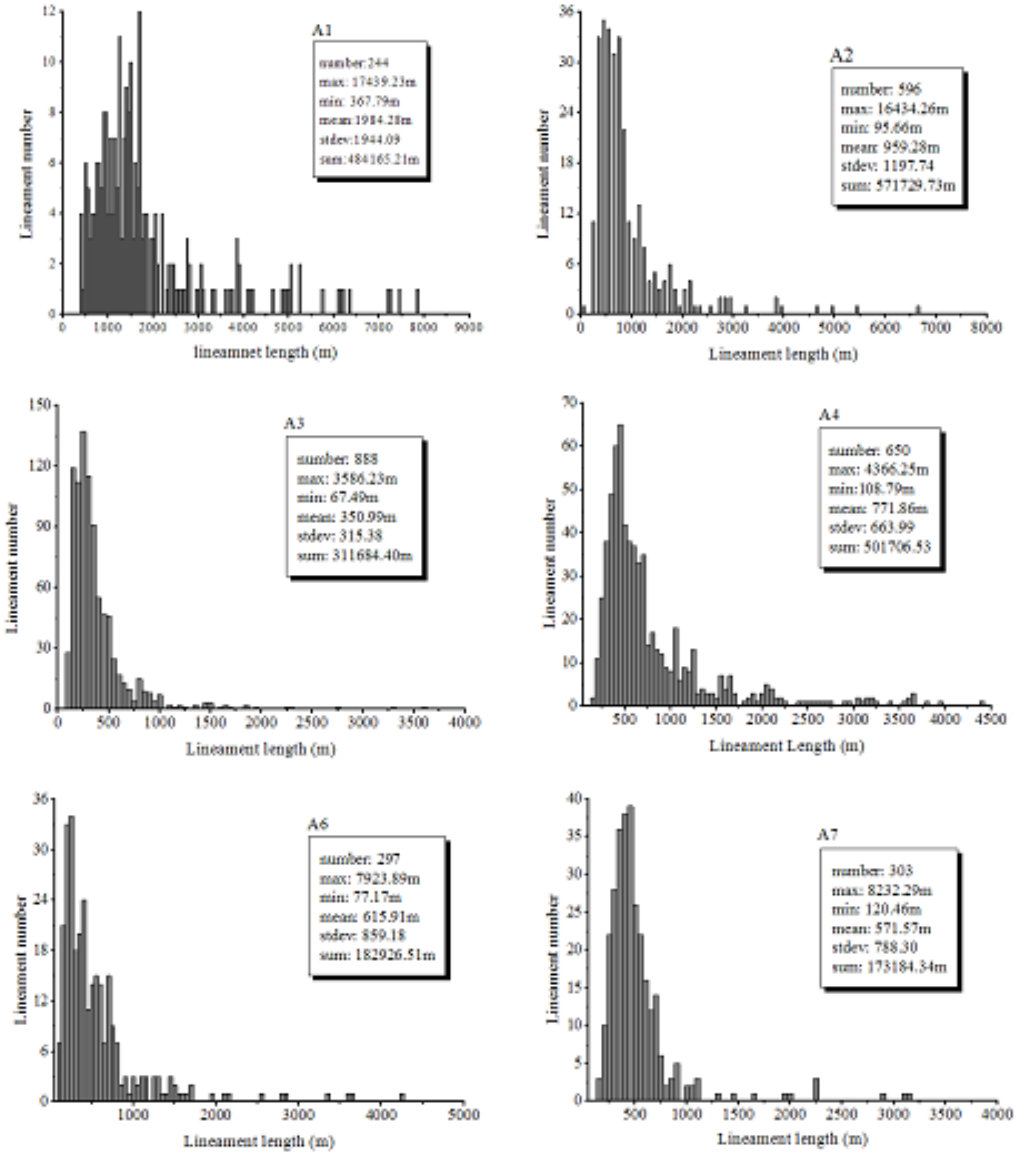

Figure 2
Histogram for lineament lengths commonly showing a lognormal distribution without a scale-dependent effect, where A5 with the same distribution is not included.

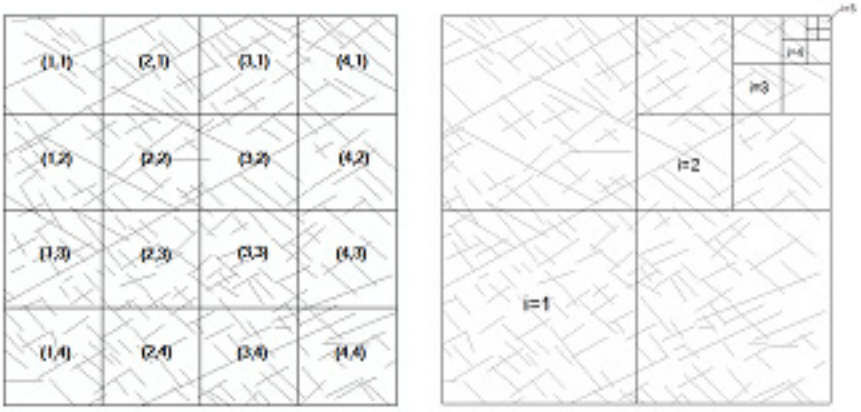

Figure 3
Equally spaced division of squared grid cells for segmenting lineaments– left: division controlled by row/column numbers; right: division by power number which automatically processes from bigger cells to smaller ones.

and numbers of lineament intersection points. Three sets of the values obtained are then computed into length density (L_d), frequency (L_f), and intersection point density (L_c), using the formulae suggested by Greenbuan (1985). The processes of lineament segmentation and lineament density computation were completed by the VBA scripts developed in ArcMap. Using the coordinates and density values extracted from the lineament file and grid file, respectively, the lineament density maps regarding L_d, L_f and L_c may be created through ordinary kriging.

Theoretically, the number of contouring maps for a targeted area can be unlimited, depending on the cell sizes and the objective of the studies (Sabins, 1999; Tripp and Vearncombe, 2004). Figure 4 presents the spatial variations of L_d, L_f and L_c in map area A7 located on the Cape Peninsula (Fig. 1b), and shows detailed density mapping using each of the above

Available on website http://www.wrc.org.za
ISSN 0378-4738 (Print) = Water SA Vol. 36 No. 3 April 2010
ISSN 1816-7950 (On-line) = Water SA Vol. 36 No. 3 April 2010

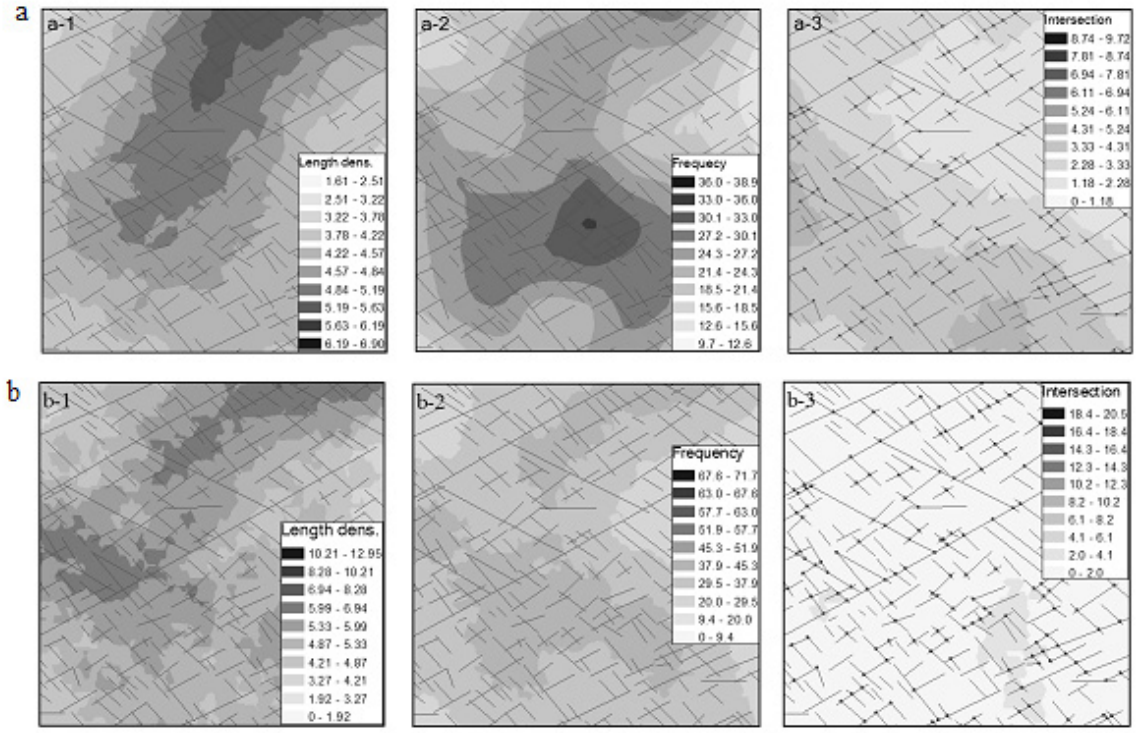

Figure 4

Example of L_d, L_f and L_c maps overlapped by lineaments and intersection points were generated with squared grids in map area A7, using the method of spherical-nugget model of ordinary kriging. a) Maps created with the cell size of 0.306 km ^{2} (556×556 m^2) which is 1.236% of the area of the map; b) Maps created with the cell size of 0.098 km ^{2} (312.5×312.5 m^2), 0.39% of the area of the map.

approaches. Cell sizes employed for the lineament segmentation and density computation are 0.306 km^2 (556×556 m^2, Fig. 4a) and 0.098 km^2 (312.5×312.5 m^2, Fig. 4b), respectively, accounting for 1.236% and 0.391% of the area (5×5 km^2) of the map. The example presented here clearly shows that the statistical patterns of lineament densities (Table 1) and the density spatial distributions are influenced by the cell sizes of a grid. In fact, more detailed analyses on the variation of lineament densities have been carried out in the domain areas A1 to A7 and the results indicate that the decrease in computing cell sizes generally increases the number of barren cells, mean density values, and the variances of lineament length densities.

Table 1
Basic statistical comparison of densities computed with various cell sizes

Density / Statistic	Length density	Frequency	Intersection point density	Cell size (km^2)	Grid points
Mean	23.040	4.415	2.840	0.309	81
Minimum	9.720	1.607	0.000		
Maximum	38.880	6.899	9.720		
Std. deviation	6.600	1.332	2.870		
Mean	33.600	5.189	0.680	0.098	256
Minimum	0.000	0.000	0.000		
Maximum	71.680	12.953	20.480		
Std. deviation	13.957	2.383	2.711		

Optimisation of representative elementary area (REA)

Above analyses of lineament densities emanate from the frequently-asked questions pertaining to the extent to which the lineament density maps are representative of study areas and whether the maps can be utilised for the evaluation of the groundwater resource at a regional scale. To answer these questions, it is necessary to determine the cell size with the best fit, namely the representative elementary areas (REA) of each domain area. Thus the relationship between lineament densities and computing cell sizes needs to be the established as the basis of REA analysis. The determination of REAs should be performed in the correct measuring dimension and by appropriate processes. As many spatial problems, similar to the above-analysed lineament densities (L_d, L_f and L_c), are scale-dependent, analysis of the scale effect of REAs is intended to assist in optimising the REAs, which in turn may improve the lineament density maps generated for the evaluation of the groundwater resource at a regional scale.

Relationship between lineament density and grid cell size

In contrast to the generation of lineament density maps in which the grid cell size has already been determined, analysis of the scale effect of lineament densities requires the establishment of a relationship between lineament density and grid cell sizes. Thus a set of computing cells with successive sizes needs to be prepared for the lineament density computations in each

domain area. Firstly, we use the grid cells as listed in Fig. 3 (left) to calculate mean lineament densities; then use concentric squared cells to calculate real densities with a size step ranging from 0.04 km^2 to 29 km^2 between 2 neighbouring cells (Fig. 5), depending on the size of the domain area. Very tiny differences in the density results from the 2 methods can be found, because both of the treatments actually produce the effect of uniform spatial distribution of the linear features. Therefore, the latter method is employed for a series of computations in domain areas A1 to A7.

Two major components of lineament densities, L_d and L_f, are computed. It is often difficult to identify lineament intersection points, especially for those intersection points near large lineaments where the termination and crossing of lineaments are not decipherable due to the effect of weathering or denser vegetation. The density of intersection points is then thought not to be representative and is discarded from the density analysis.

The calculated lineament density results of the domain areas for L_d, L_f, corresponding squared cell size and the side length of each cell are listed in Table 2; note that Area A3 has been split into 2 subset areas viz. A3-1 and A3-2, considering some areas of uneven distribution of the lineaments. Based on these data, the relationship of lineament density and frequency with computing cell size (s) can be summarised without exception by a power law (Fig. 6) and is expressed as follows:

$$L_{d(f)} = a \cdot s^{-b}, \quad a > 0, b > 0 \tag{1}$$

where:

$L_{d(f)}$ is the combined expression of lineament length density (L_d) and frequency (L_f) constants a and b are different from one domain area to another.

Accordingly, the relation of L_d and L_f to side length (l) of squared cells may be established as:

$$L_{d(f)} = a \cdot l^{-2b} \tag{2}$$

Factors influencing REA

The density-cell size plots in Fig. 6 give the potential to determine the minimum cell size (REA) at which the density values remain relatively stationary along with the increase in cell sizes, because of the shapes of the power law curves. Currently, methods of determining the REAs are mostly dependent on visual analysis derived from the density-cell size diagrams. This would certainly lead to a large bias in the estimated REAs due to the differences in:

- Size step of grid cells
- Measuring dimensions (e.g. length or area of grid cells)
- Measured parameters (e.g. L_d and L_f) which may produce different REAs that are respectively regarded as lower and upper limits of the REAs

Strictly speaking, an estimate of REAs should be in units of area (*2D: L*^{2}) to keep the dimension consistent. However, almost all previous studies have used units of length (dimension: *L*) to estimate the REAs, perhaps because it is easier to use units of length for rectangle cells, or radii for circular cells, rather than units of area, to control the equally-spaced density computations. In practice, if there exists only a linear relationship between lineament densities and measuring dimensions, units of length can be used to measure the size of REAs; in all other instances it is rarely practical. This is highlighted by the following derivatives of Eqs. (1) and (2) for the problem of function convergences:

1st derivative:

$$\frac{\partial L_{d(f)}}{\partial s} = -abs^{-(b+1)}; \quad \frac{\partial L_{d(f)}}{\partial l} = -2abl^{-(2b+1)} = -2abs^{-(b+1/2)} \tag{3}$$

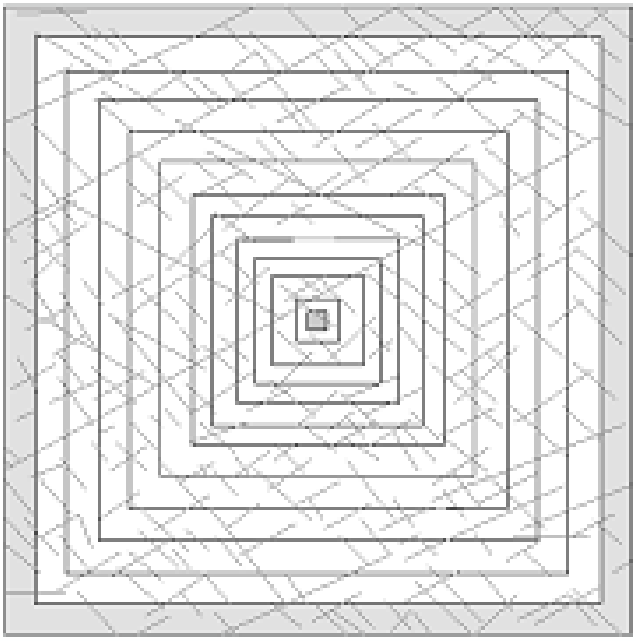

Figure 5
A set of concentric squared cells for the computation of lineament densities

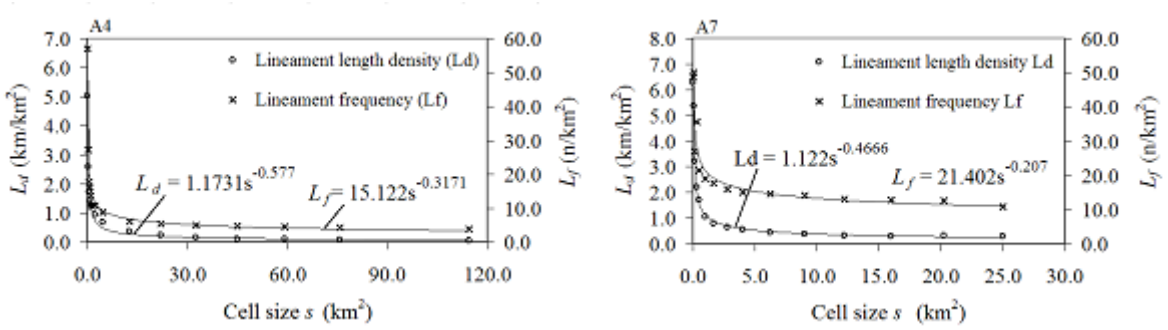

Figure 6
Plots of lineament length density and frequency against cell size in areas A4 and A7 as the examples of 7 domain areas, which show a universal relation expressed by a negative power function, in the TMG areas (see Table 2).

Available on website http://www.wrc.org.za
ISSN 0378-4738 (Print) = Water SA Vol. 36 No. 3 April 2010
ISSN 1816-7950 (On-line) = Water SA Vol. 36 No. 3 April 2010

Available on website http://www.wrc.org.za
ISSN 0378-4738 (Print) = Water SA Vol. 36 No. 3 April 2010
ISSN 1816-7950 (On-line) = Water SA Vol. 36 No. 3 April 2010

Table 2
Lineament length density (L_d) and frequency (L_f) computed by concentric squared grid cells with various sizes in domain areas (A1 to A7)

A1	Cell s (km²)	0.640	1.778	2.778	4.592	9.000	16.000	25.000	36.000	49.000	64.000	81.000	100.00	121.00	144.00	169.00	196.00	225.00			
	Length (km)	0.800	1.333	1.667	2.143	3.000	4.000	5.000	6.000	7.000	8.000	9.000	10.000	11.000	12.000	13.000	14.000	15.000			
	L_d(km/km²)	1.25	0.94	0.81	0.60	0.46	0.36	0.30	0.25	0.24	0.21	0.17	0.15	0.15	0.14	0.12	0.10	0.09			
	L_f(n/km²)	6.25	2.81	1.80	1.74	1.67	1.63	1.76	1.81	1.69	1.59	1.54	1.47	1.38	1.28	1.26	1.20	1.08			
A2	Cell s (km²)	0.071	0.118	0.230	0.360	0.640	1.778	2.939	5.760	9.000	16.000	25.000	36.000	42.250	49.000	56.250	64.000	72.250	81.00	121.00	144.00
	Length (km)	0.267	0.343	0.480	0.600	0.800	1.333	1.714	2.400	3.000	4.000	5.000	6.000	6.500	7.000	7.500	8.000	8.500	9.00	11.00	12.000
	L_d(km/km²)	3.75	3.25	2.91	2.48	1.91	0.90	0.64	0.49	0.43	0.25	0.16	0.20	0.18	0.18	0.18	0.17	0.15	0.13	0.11	0.10
	L_f(n/km²)	14.06	17.01	8.68	13.89	9.38	6.75	7.83	5.56	5.33	4.31	3.92	3.81	3.74	3.78	3.75	3.63	3.60	3.42	3.12	2.83
A3-1	Cell s (km²)	0.014	0.023	0.045	0.124	0.401	0.746	1.114	1.842	3.610	10.028	14.188	17.361	24.668	36.000						
	Length (km)	0.117	0.151	0.211	0.352	0.633	0.864	1.056	1.357	1.900	3.167	3.767	4.167	4.967	6.000						
	L_d(km/km²)	5.91	5.89	5.13	3.51	1.58	1.05	1.03	0.64	0.48	0.16	0.16	0.17	0.13	0.11						
	L_f(n/km²)	218.09	131.93	67.31	48.47	34.90	30.84	24.23	24.98	22.16	17.45	16.14	16.30	16.46	15.08						
A3-2	Cell s (km²)	0.008	0.016	0.045	0.124	0.205	0.401	1.114	2.741	4.225	8.154										
	Length (km)	0.090	0.127	0.211	0.352	0.452	0.633	1.056	1.656	2.056	2.856										
	L_d(km/km²)	12.31	9.58	6.29	4.44	3.20	1.85	0.79	0.74	0.51	0.37										
	L_f(n/km²)	122.16	62.33	44.88	56.54	43.98	37.40	23.34	22.62	20.35	17.05										
A4	Cell s (km²)	0.053	0.184	0.396	0.677	0.946	1.413	2.337	4.580	12.721	22.090	32.490	44.890	59.290	75.690	114.49					
	Length (km)	0.229	0.429	0.629	0.823	0.973	1.189	1.529	2.140	3.567	4.700	5.700	6.700	7.700	8.700	10.700					
	L_d(km/km²)	5.03	2.59	1.73	1.42	1.29	1.22	0.93	0.68	0.37	0.25	0.15	0.10	0.10	0.08	0.06					
	L_f(n/km²)	57.00	27.12	17.67	16.24	13.74	10.61	10.70	8.73	6.05	5.39	5.05	4.79	4.57	4.32	3.83					
A5	Cell s (km²)	0.037	0.052	0.077	0.128	0.250	0.694	1.000	2.250	4.000	6.250										
	Length (km)	0.192	0.227	0.278	0.357	0.500	0.833	1.000	1.500	2.000	2.500										
	L_d(km/km²)	3.99	3.61	3.43	3.21	2.52	1.62	1.37	1.04	0.72	0.49										
	L_f(n/km²)	81.12	77.44	51.84	39.20	28.00	21.60	21.00	19.11	16.75	15.04										
A6	Cell s (km²)	0.026	0.071	0.198	0.327	0.640	1.778	2.250	4.000	6.250	9.000	12.250	16.000								
	Length (km)	0.160	0.267	0.444	0.571	0.800	1.333	1.500	2.000	2.500	3.000	3.500	4.000								
	L_d(km/km²)	5.79	3.69	3.01	2.46	1.76	0.80	1.00	0.73	0.61	0.52	0.40	0.36								
	L_f(n/km²)	78.13	56.25	35.44	24.50	18.75	16.88	16.89	14.25	13.76	14.00	14.29	14.13								
A7	Cell s (km²)	0.020	0.040	0.111	0.309	0.510	1.000	1.690	2.778	4.000	6.250	9.000	12.250	16.000	20.250	25.000					
	Length (km)	0.143	0.200	0.333	0.556	0.714	1.000	1.300	1.667	2.000	2.500	3.000	3.500	4.000	4.500	5.000					
	L_d(km/km²)	6.27	5.37	3.23	2.21	1.71	1.08	0.79	0.64	0.57	0.44	0.38	0.31	0.29	0.32	0.30					
	L_f(n/km²)	49.00	50.00	27.00	35.64	21.56	19.00	17.75	15.84	15.00	14.72	14.22	13.14	12.94	12.59	10.92					

2nd derivative:

$$\frac{\partial^2 L_{d(f)}}{\partial s^2} = ab(1+b)s^{-(b+2)}\ ;\ \frac{\partial L^2{}_{d(f)}}{\partial l^2} = 2ab(1+2b)l^{-2(b+1)}$$

$$= 2ab(1+2b)s^{-(b+1)} \quad (4)$$

From the above 2 equations, it is clear that at a same-size level the convergence of densities is not consistent with the relation of the length (l) and the area (s), namely, $s = l^2$. This implies that the determination of REAs by means of units of length versus units of area may yield different results in a non-linear spatial problem.

Table 3 summarises the influences of the 3 factors on REA estimation by changing the density value to less than 10% in 3 successive measuring points. The example shows that a trend of increasing REAs with increasing size steps is predominant, regardless of measuring dimension and type of lineament densities. At a same-size level, REAs measured in length units are much larger than those measured in area units, which can be distinguished from the slopes of density values against the 2 scales presented in Eq. (3), where the drop of curve slope against length is twice as much as that against area. A wide range of REAs exists between those from L_d and L_f, in which the L_d generally appears to produce an upper limit, and L_f a lower limit, of REAs. Clearly, these will make ultimate determination of REAs extremely difficult for each domain area if the effects of cell-size step, measuring dimension, and parameters L_d and L_f on the REAs are not removed.

Table 3
Comparisons of REAs with the influence of 3 factors

Measuring dimension	Size step	REA (km²) in A4		REA (km²) in A7	
		L_d	L_f	L_d	L_f
s (km²)	0.04	0.33	0.21	0.37	0.29
	0.10	0.81	0.51	0.62	0.40
	0.20	1.61	1.01	1.41	0.82
l(m)	100	1.96	0.81	1.44	0.64
	200	7.29	2.89	5.29	1.69
	300	18.49	6.25	11.56	3.61

Determination of REA

In view of the influence of the above-mentioned factors and the relationship between lineament densities and computing cell sizes on REA estimation, a new method based on regression analyses is proposed and applied to the determination of REA with the objective of determining a consistent REA for each domain area (A1 to A7). The least-squares method associated with linearisation of nonlinear relationships has been extensively applied to many fields of geosciences, for which the coefficient of determination (R^2) or correlation coefficient (R) is most commonly used to assess correlativity of 2 sets of observations. In the case presented in Table 2, the correlations of L_d–s and L_f–s can be expected as negative power relations, which are modelled by Eq. (1). Before applying the negative power models to the determination of REAs, the following 2 preconditions should be considered:

- Only area (s) scale can be used to estimate REAs
- Only the equally-spaced dataset can be used to determine REAs

To enhance the applicability of REAs, a comprehensive method of determining the REAs needs to be proposed through the combined lineament density derived from L_d and L_f jointly, instead of from L_d and L_f separately. For this purpose, the photolineament factor method suggested by Hardcastle (1995) is adapted, which, alternatively, can be expressed as:

$$L_{df} = c_1 L_d + c_2 L_f \quad (5)$$

where:

L_{df} is the combined lineament density from length density and frequency independently weighted by constants c_1=0.6 and c_2=0.4, respectively.

Note that the L_d and L_f should be normalised before they are added, in order to ensure that different unit datasets are independent of the unit of measurement. The empirical constants c_1 and c_2 can be obtained through simulation and calibration.

Based on the existing data listed in Table 2, the normalised L_d and L_f do not alter the patterns of their relationship with cell sizes as shown in Fig. 7, where the L_{df} is also plotted and its graph falls between the former two. The regression expressions of L_{df} –s listed in Fig. 7, with the coefficient of determination (R^2) of more than 0.97, indicate very high correlations between combined lineament densities and cell sizes. Therefore, these expressions of combined lineament densities can be used to estimate the REA for each domain area.

The last step is to establish a convergence criterion by means of which the REAs may be ultimately identified. Because the 2nd derivative of each power function listed in Fig. 7 never reaches zero by any cell-size values, we cannot use Eq. (4) to be the algorithm in determining the REAs. In order to ensure that the absolute difference of 2 consecutive density values is small enough, therefore, the condition of 1st derivative of L_{df} equalling -0.0175 (or when the curve slope equals 1º) is specified to be the convergence criterion for REA. It can be shown that, under this condition with a size step of 0.04 km², the absolute error of 2 consecutive density values for each expression is not more than 0.0007 where the REA is given.

Table 4 summarises the REAs resulting from a series of calculations with the convergence criterion of curve slope not more than 1º based on the formulae listed in Fig. 7. REAs range between 2.39 km² and 7.37 km², with an average of 3.94 km², while the side length of REAs ranges between 1 545.11 m and

Table 4
REAs in the TMG areas resulted from combined densities

Domain area	REA (km²)	REA side length (m)	Size of domain area (km²)	REA percentage (%)
A1	7.37	2 714.47	225.00	3.27
A2	4.74	2 177.18	144.00	3.29
A3-1	2.59	1 610.69	36.00	7.21
A3-2	2.39	1 545.11	9.00	26.53
A4	3.58	1 893.12	114.50	3.13
A5	3.93	1 983.44	6.25	62.94
A6	3.39	1 840.95	16.00	21.18
A7	3.50	1 870.48	25.00	13.99
Average	3.94	1 954.43	71.97	17.69
SD	1.57	365.96	80.47	20.32

Available on website http://www.wrc.org.za
ISSN 0378-4738 (Print) = Water SA Vol. 36 No. 3 April 2010
ISSN 1816-7950 (On-line) = Water SA Vol. 36 No. 3 April 2010

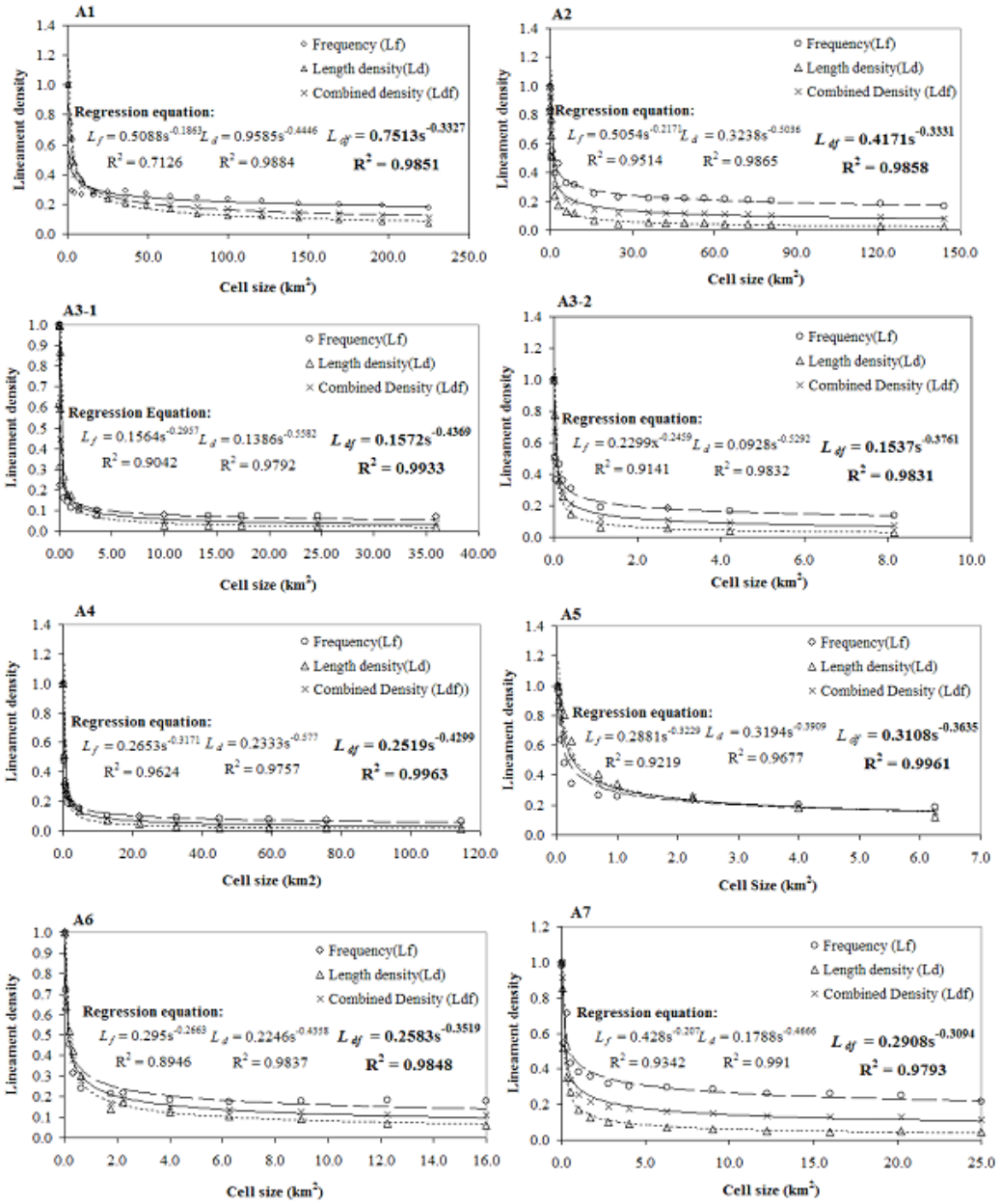

Figure 7
Relationship of cell size with normalised lineament length density, frequency, and consequently combined lineament density of the 8 areas (A1 to A7), which follow a negative power law. The densities with each regression equation and correlation coefficient show very high correlativity between s and L_f, L_d and L_{df}.

2 714.47 m. The REA percentage of each domain area fluctuates between 3.13% and 62.94% with a mean value of 17.69%. Moreover, without exception, the bigger REA percentage accompanies the smaller domain area, which actually implies the scale effect of REAs, as will be discussed later.

As can be seen from the above analyses, the construction of combined lineament density has many advantages in determining REAs. Besides, based on a comprehensive consideration of different types of densities, the elimination of the density dimension effect through normalisation may contribute to many spatial problem analyses such as factor superposition and objective overlay.

Two examples of combined density in Areas A3 and A4 (with their REAs listed in Table 4) are plotted in Fig. 8, showing that when grid cell sizes are near and over REA the difference in density statistics and shapes of spatial distributions may become very small. This makes the density map potentially valuable for the evaluation of groundwater studies when it is incorporated with other relevant maps.

However, caution should be exercised when utilising the density map for analysis of the spatial problem, not only because of the above-mentioned lineament densities but also because their consequent REAs are scale-dependent. The validity of lineament densities depends on the grid cell sizes involved (Fig. 7) at a domain-area scale. The reliability of an REA is dependent on the size of the domain area (Fig. 9) at a study-area scale.

Figure 9 is plotted from the data listed in Table 4, which shows a linear relationship between REA and the size of the domain area (S), with the correlation coefficient of 0.867:

$$REA = 0.0169S + 2.7424 \quad (6)$$

This linear relation provides an important tool to estimate REAs for the domain areas with various sizes. It appears to give the lower limit of REA as 2.74 km² at the curve intercept point where the size of domain area is nil. Because the smallest domain area in the study is 6.25 km², the lower limit of REA can therefore be regarded as a range of 2.39 to 2.85 km² (see Table 4 and Fig. 9).

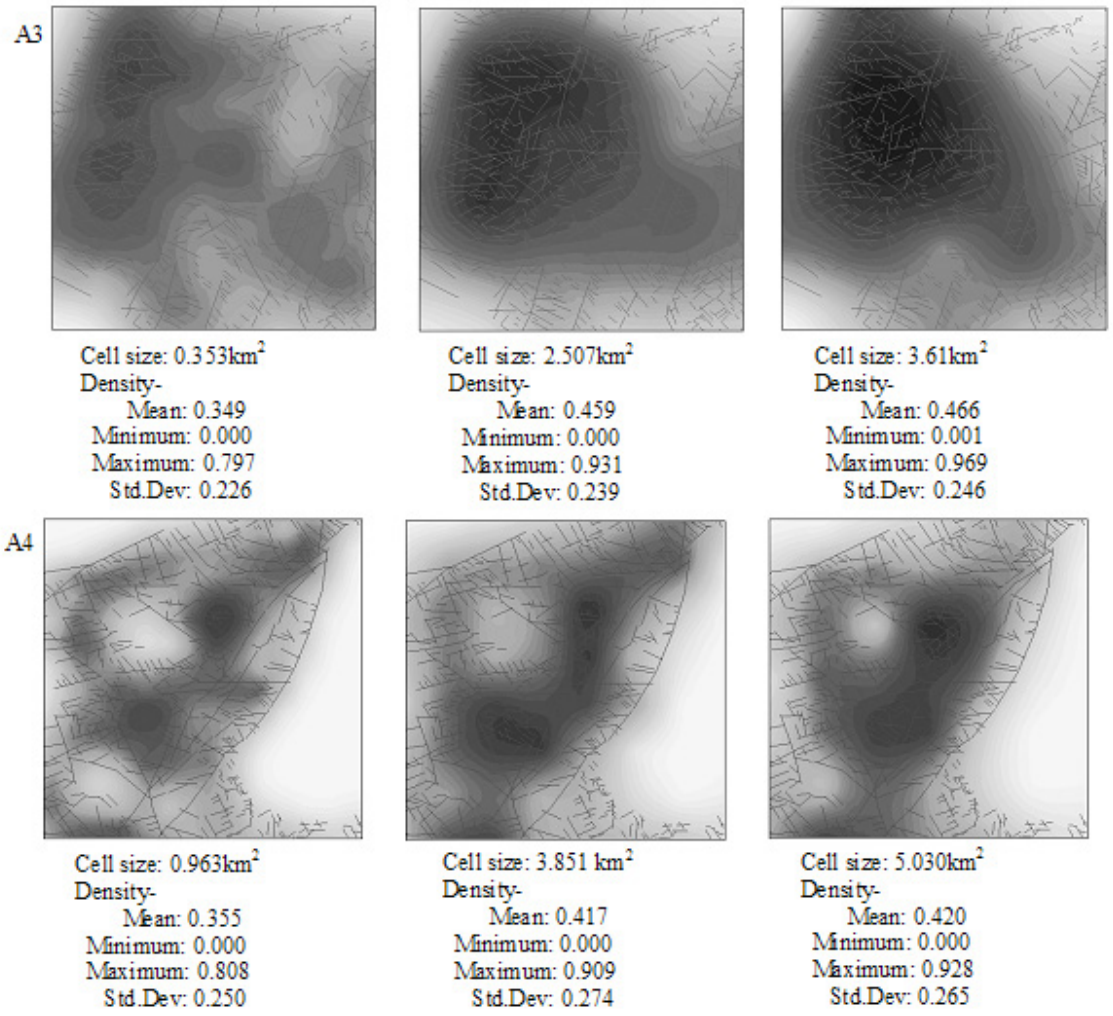

Figure 8

Combined lineament density plotted with various cell sizes in domain areas A3 (REA=2.49 km²) and A4 (REA=3.58 km²), where the cell size is close to REA in the middle of each.

When considering the REA percentages in the study area with the 7 domain areas involved, it is interesting to note that the relationship between REA percentage (%REA) and domain-area size (S) has a similar power law relationship to that of lineament densities, which can be expressed as:

$$\%REA = 199.94S^{-0.8261}, \quad (R = 0.973) \tag{7}$$

When generating a lineament density map, it should be noted that a significant domain-area size of more than 40 km² is preferable for the generation of a lineament map, because the higher REA percentage of the smaller domain area will produce fewer grid points which make the density map meaningless.

In order to optimise lineament density mapping, our study determined %REA with the best fit for the study area, as well as the corresponding domain-area size. Based on Eq. (7), the same method of determining REA for each domain area can be used by means of curve-fitting techniques, using the same convergence criterion. As a result, the REA percentage with the best fit in our study area is 3.33% of the corresponding domain-area size of 150.43 km². This means that, at the study-area scale, a domain area with a size of more than 150 km² will produce a constant REA percentage of 3.33% (e.g. 5.01 km² of REA for 150 km² of domain-area size) by means of which the upper limit of REA can be estimated.

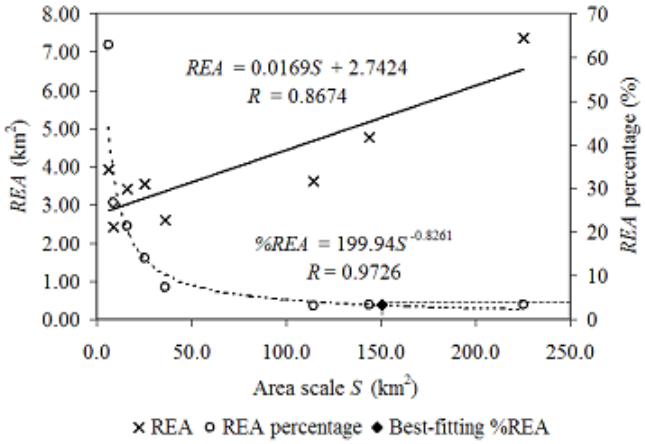

Figure 9

Relationship of REA and REA percentage with area scale based on Table 4, showing a linear and a negative power relation, respectively

Available on website http://www.wrc.org.za
ISSN 0378-4738 (Print) = Water SA Vol. 36 No. 3 April 2010
ISSN 1816-7950 (On-line) = Water SA Vol. 36 No. 3 April 2010

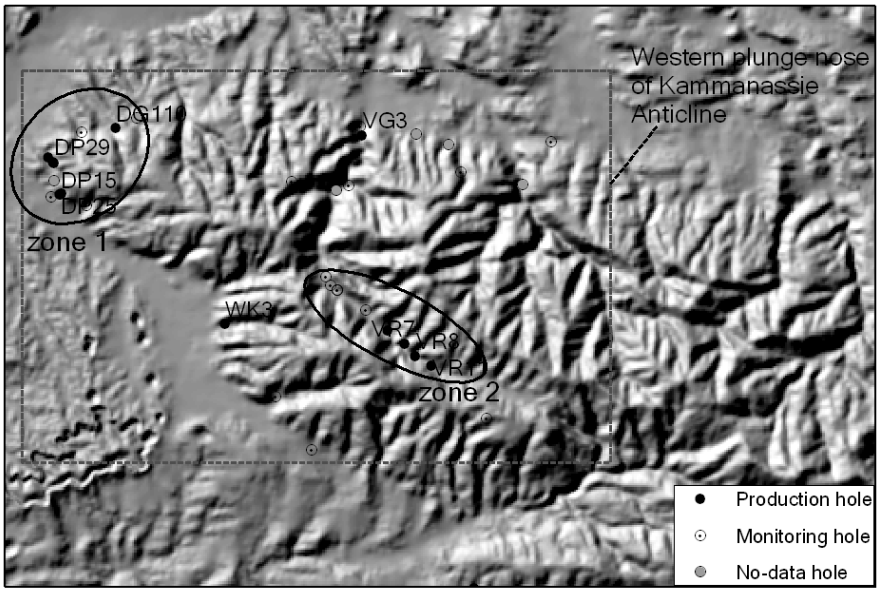

Figure 10
Map of study area in the west plunge nose of the Kammanassie anticline showing the location of Vermaaks River well field (zone 2) and Varkieskloof and Bokkraal well fields (Zone 1) developed in the 1990s.

Applicability of REA and combined lineament density

Considering the characteristic of spatial variation of lineament densities, it can be argued that lineament density maps produced with smaller grid cells may help to study more localised problems. The smaller grid cells often produce many higher density zones in a study area, which can provide multiple options for relevant objectives but at the same time could make the targeting decision very difficult. In general, for the scaling-up problems with a single target zone involved, the REA approach can be used to determine the keystone zone in an area. However, further research is required to assess the potential of the developed REA combined with lineament density, and generation of its corresponding density map, to be extrapolated to other TMG areas.

Lineament densities and corresponding density maps are valuable in many fields of groundwater studies. In terms of the application of lineament density, Edet et al. (1998) have established the slight to moderate correlations of L_d with borehole water temperature and conductivity, well yield, aquifer transmissivity, and longitudinal conductance. In the study of groundwater in a karstified area of Vietnam, Tam et al. (2004) used the incept point of 2 curves of L_d –s and L_f –s to obtain the REA, from which they constructed the relationship between L_d and borehole specific capacity, by using cluster analysis. Lineament maps, when integrated with maps of geomorphology, slope, drainage density, and regional water level through factor superposition techniques, are very useful for targeting potentially high groundwater recharge areas (Shankar and Mohan, 2005).

Figure 10 shows the geomorphic feature and location of 2 well fields (Zone 1 and Zone 2) on the western plunge nose of the Kammanassie anticline consisting of a continuous sequence of the TMG sandstones, 30 km east of Oudtshoorn, Western Cape. The well fields in the area are a vital part of Little Karoo Rural Water Supply Scheme. During 1993 to 2003, 49.07% of annual 1.1×10^6 m^3 of groundwater had been abstracted from Vermaaks River well field (Zone 2), while the groundwater extracted from Varkieskloof and Bokkraal well fields (Zone 1 in Fig. 10) comprised some 19% of the annual amount. Due to the lowering of the water level, 8 production boreholes in Zone 1 have been reduced to no more than 4, while 5 holes in Zone 2 are operational but their abstraction rate has been reduced as well. The hydrogeological condition of the area has been discussed in detail by Hälbich and Greef (1995), Kotze (2002), and Wu (2005). In particular, lineament mapping and interpretation of the Kammanassie area has been carried out by Kotze (2002). The lineament data provided a comprehensive presentation of the dominant fracture system, which indicates that the dominant striking fractures are E-W, N-S, NNW-SSE, and NE-SW, and the latter two are conjugate fracture sets.

Based on Kotze's lineament data, the western plunge nose area (dashed rectangle in Fig. 10) of the Kammanassie anticline is chosen as the case-study area for the application of lineament densities. As the size of the area is 150 km^2, the REA percentage based on Eq. (7) is 3.033%. Using rectangle grid cells with a size of 4.2 km^2, close to the REA of 4.78 km^2, lineament length density, frequency, and combined lineament density can be computed, which are presented in Fig. 11. The maps of lineament length density, frequency, and combined lineament density simultaneously show that only one zone of higher density exists. This probably indicates the keystone zone of groundwater occurrence; however, the lower density does not mean that there is no groundwater occurrence in the area (Table 5). In fact, if there are multiple options for targeting zones associated with the spatial variation of lineament densities, the REA approach provides a powerful tool to sort out the first selectable one. Moreover, considering aforementioned factors that influence REA and the advantages of combined lineament density, the information from the combined lineament density map is hence recommended for the use of relevant groundwater evaluation.

Conclusion

The study has put forward a universal approach for the determination of an optimal REA with application in TMG area through lineament density analyses, which in turn may improve the quality of lineament density maps and their application to the evaluation of groundwater resources at a regional scale.

With the rapid development of high-resolution remote sensing data and GIS technologies, it is now feasible to quantify the imagery for multiple objectives at various scales. A properly prepared lineament density map originated from the imagery

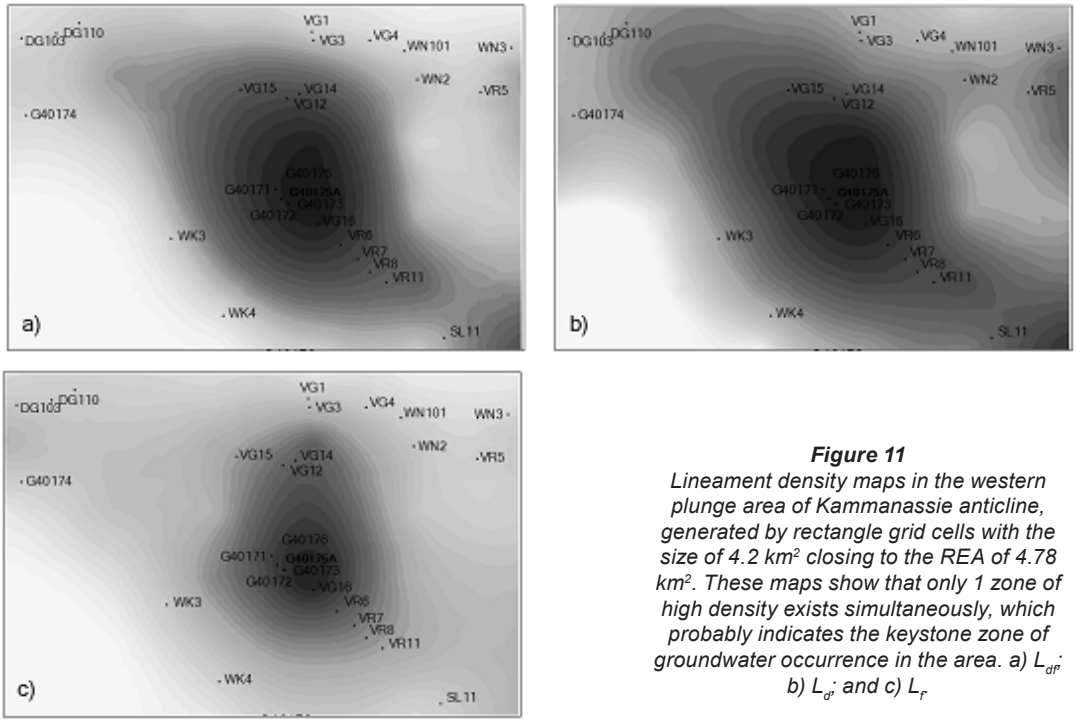

Figure 11
Lineament density maps in the western plunge area of Kammanassie anticline, generated by rectangle grid cells with the size of 4.2 km² closing to the REA of 4.78 km². These maps show that only 1 zone of high density exists simultaneously, which probably indicates the keystone zone of groundwater occurrence in the area. a) L_{df}; b) L_d; and c) L_r

Table 5
Comparison between lineament density and borehole blow yield and recommended yield

Borehole No.	Type	Depth (m)	Blow yield (ℓ/s)	Recommended abstraction (ℓ/s)					L_{df}	Mean L_{df}	Map location
				1992	1993	1998	2000	Subtotal			
DP10	P	210	7.0	14.3	4.5	–	2.0	13.0	0.261	0.243	Zone 1
DP12	P	192	20.0				3.0		0.223		
DP29	P	240	4.0				3.0		0.215		
DP25	P	203	20.0	9.8	–	7.0	3.0		0.269		
DG110	P	212	7.5				2.0		0.256		
DG103	M	250	5.7						0.231		
VG3	P	206.7	12.0				3.0	3.0	0.320	0.285	North border
VG4	M	113	<2.0						0.249		
VR6	P	250	15		8.0		2.5	22.5	0.766	0.721	Zone 2
VR7	P	177	23.0	19.7	20.0	11.0	10.0		0.667		
VR8	P	251.3	13.0	9.8	10.0	8.0	5.0		0.602		
VR11	P	224.5	20.0		8.0	6.0	5.0		0.552		
G40171	M	50							0.896		
G40172	M	10	5.0						0.931		
G40173	M	10	3.0						0.933		
G40174	M	147	13.0						0.228		
G40175A	M	84	11.75	Artesian flow: 11.7					0.917		

Note: P– production hole; M – monitoring hole. Recommended abstraction of boreholes is after Jolly (2002) and Kotze (2002)

interpretation can be applied to many fields of groundwater studies for spatially-correlated problems, when used with other relevant map sources. However, analysis of the lineament densities frequently encounters problems as to whether the density maps are representative of an area and whether the map can ultimately be used to evaluate groundwater resources at a regional scale. This is because the computed lineament densities are scale-dependent with regard to both the size of the computing grid cells and the size of the domain areas. Thus the main objective of the study was to determine the REAs with the best fit for both domain area and the study area comprising several domain areas.

To improve the constancy of the determination of REAs, methods based on curve-fitting techniques were developed, in which the lineament density is represented by combined lineament density jointly derived from lineament length density and frequency. For the evaluation of spatially heterogeneous problems, it is recommended that the combined lineament density be used, rather than using length density or frequency separately, due to consideration of the density dimension effect. The

Available on website http://www.wrc.org.za
ISSN 0378-4738 (Print) = Water SA Vol. 36 No. 3 April 2010
ISSN 1816-7950 (On-line) = Water SA Vol. 36 No. 3 April 2010

density analysis result showed that a universal power law relationship exists between the lineament densities and computing cell sizes, from which the optimal REA for each domain area could be precisely determined by area dimension (L^2) instead length dimension (L). Based on the power law relationship, the convergence criterion of a curve slope of no more than 1º provides a more convenient and accurate way to determine the REA of each domain. Moreover, when the determined REAs and their corresponding domain areas are plotted together, the REA scale effect can be observed. Optimal REAs for the entire study area should therefore be determined, not by simply averaging the REAs of the domain areas, but from the linear relationship between the REA and the size of the domain area or the power law relationship between REA percentage and the size of domain area, by means of the curve-fitting technique.

Acknowledgements

The authors are grateful to the Water Research Commission (WRC) of South Africa for providing financial support for the study and permission to publish the data. Professor Yongxin Xu of the University of the Western Cape is gratefully acknowledged for his constructive comments that have greatly enhanced the manuscript. Revision and comments from the editors and reviewers are greatly appreciated. The University of Fort Hare is also acknowledged for providing all the research opportunities when the authors were working there.

Reference

BEAR J (1972) *Dynamics of Fluids in Porous Media*. Elsevier, New York. 764 pp.

BEVEN KJ, WOOD EF and SIVAPALAN M (1988) On hydrological heterogeneity – catchment morphology and catchment response. *J. Hydrol.* **100** 353-375.

BRACQ P and DELAY F (1997) Transmissivity and morphological features in a chalk aquifer: a geostatistical approach of the relationship. *J. Hydrol.* **191** 139-160.

BRESSAN MA and ANJOS CD (2003) Techniques of remote sensing applied to the environmental analysis of part of an aquifer located in the São José Dos Campos region SP, Brazil. Environ. *Monit. Assess.* **84** 99-109.

BYGAART AV and PROTZ R (1999) The representative elementary area (REA) in studies of quantitative soil micromorphology. *Geoderma* **89** 333-346.

CASAS AM, CORTES, AL, MSESTRO A, SORIANO MA, RIAGUAS A and BERNAL J (2000) LINDENS: A program for lineament length density analysis. *Comp. Geosci.* **26** 1011-1022.

DE BEER CH (2001) The Stratigraphy, Lithology and Structure of the Table Mountain Group. In: Pietersen K and Parsons R (eds.) A Synthesis of the Hydrogeology of the Table Mountain Group – Formation of a Research Strategy. WRC Report No. TT 158/01. Water Research Commission, Pretoria, South Africa. 9-18.

DEGNAN JR and CLARK SF (Jr.) (2002) Fracture-Correlated Lineaments at Great Bay. Southeastern New Hampshire, US Geological Survey Open-File Report 02-13. 14 pp.

DRURY SA, PEART RJ and DELLER ME (2001) Hydrogeological potential of major fractures in Eritrea. *J. Afr. Earth Sci.* **32** 163-177.

EDET AE, OKEREKE CS, TEME SC and ESU EO (1998) Application of remote-sensing data to groundwater exploration: A case study of the Cross River State, southwestern Nigeria. *Hydrogeol. J.* **6** 394-404.

GREENBUAN D (1985) *Review of Remote Sensing Applications to Groundwater Exploration in Basement and Regolith*. British Geological Survey Report OD 85/8. 36 pp.

GUSTAFSSON P (1994) Spot satellite data for exploration of fractured aquifers in a semi-arid area in southeastern Botswana. *Appl. Hydrogeol.* **2** 9-18.

HÄLBICH IW and GREEF GJ (1995) Final report on a structural analysis of the west plunge nose of the Kammanassie anticline. Technical report to the Department of Water Affairs, South Africa.

HARDCASTLE KC (1995) Photolineament factor: a new computer aided method for remotely sensing the degree to which Bedrock is fractured. *Photogrammetric Engin. Remote Sensing.* **61** (6) 739-747.

JOLLY JL (2002) Sustainable use of Table Mountain Group aquifers and problems related to scheme failure. In: Pietersen K and Parsons R (eds.) A Synthesis of the Hydrogeology of the Table Mountain Group – Formation of a Research Strategy. WRC Report No. TT 158/01. Water Research Commission, Pretoria, South Africa. 108-111.

KIM GB, LEE JY and LEE KK (2004) Application of representative elementary area (REA) to lineament density analysis for groundwater implications. *Geosci. J.* **8** (1) 27-42.

KOCH M and MATHER PM (1997) Lineament mapping for groundwater resource assessment: a comparison of digital synthetic aperture (SAR) imagery and stereoscopic large format camera (LFC) photographs in the Red Sea Hills, Sudan. *Int. J. Remote Sensing* **18** 1465-1482.

KOTZE JC (2002) Toward a Management Tool for Groundwater Exploitation in the Table Mountain Sandstone Fractured Aquifer. WRC Report No.729/1/02. Water Research Commission, Pretoria, South Africa. 147 pp.

KRESIC N (1995) Remote sensing of tectonic fabric controlling groundwater flow in Dinaric Karst. *Remote Sensing Environ.* **53** 85-90.

KULATILAKE PHSW and PANDA BB (2000) Effect of rock block and joint geometry on jointed rock hydraulics and REV. *ASCE J. Eng. Mech.* **126** (8) 850-858.

MABEE SB, HARDCASTLE KC and WISE DW (1994) A method of collecting and analyzing lineaments for regional-scale fractured bedrock aquifer studies. *Ground Water* **32** 884-894.

McCARTHY T and RUBIDGE B (2005) *The Story of Earth and Life, a South African Perspective on a 4.6-billion-year Journey*. New Holland Publishing (South Africa). 184-211.

MOSTAFA ME and QARI MY (1995) An exact technique of counting lineaments. *Engin. Geol.* **39** 5-16.

O'LEARY DW, FRIEDMAN JD and POHN HA (1976) Lineament, linear, lineation: some proposed new word standards for old terms. *Geol. Soc. Amer. Bull.* **87** 1463-1469.

OWEN R, MIKAILHOV A and MAZITI A (2003) Groundwater occurrence in crystalline basement aquifers a GIS based study of a borehole dataset in a uniform granitic terrain in southern Zimbabwe. *Proc. 4th Waternet/Warfsa Symposium, 15 to 17 October 2003, Gaberone, Botswana*. 1-11.

RODELL M and FAMIGLIETTI JS (2002) The potential for satellite-based monitoring of groundwater storage changes using GRACE: the High Land Plains aquifer, Central US. *J. Hydrol.* **263** 245-256.

RUST IC (1973) The evolution of the Palaeozoic Cape Basin, southern margin of Africa. In: Nairn AEN and Stehli FG (eds.) *The Ocean Basins and Margins,* Vol. 1. The South Atlantic Plenum, New York. 247-276.

SABINS FF (1999) Remote sensing for mineral exploration. *Ore Geol. Rev.* **14** 157-183.

SANDER P, CHESKEY MM and MINOR TB (1996) Groundwater assessment using remote sensing and GIS in a rural groundwater project in Ghana: lesson learned. *Hydrogeol. J.* **4** (3) 40-49.

SANDER P, MINOR TB and CHESLEY MM (1997) Groundwater exploration based on lineament analysis and reproducibility tests. *Ground Water* **35** 888-894.

SCHOWENGERDT R, BABOCK EM, EHTRIDGE L and GLASS CE (1979) Correlation of geologic structure inferred from computer enhanced Landsat imagery with underground water supplies in Arizona. In: Deutsch M, Wiesnet DR and Range A (eds.) *Satellite Hydrology:* 387-397. *Proc. 5th W.T. Pecora Memorial Symposium on Remote Sensing, 10 to 15 June 1979,* Sioux Falls, South Dakota, American Water Resources Association.

SHANKAR MNR and MOHAN G (2005) A GIS based hydrogeomorphic approach for identification of site-specific artificial-recharge techniques in the Deccan Volcanic Province. *J. Earth Syst. Sci.* **114** (5) 505-514.

TAM VT, SMEDT FD, BATELAAN O and DASSARGUES A (2004) Study on the relationship between lineaments and borehole specific capacity in a fractured and karstified area in Vietnam. *Hydrogeol. J.* **12** 662-673.

TRIPP GI and VEARNCOMBE JR (2004) Fault/fracture density and mineralization: a contouring method for targeting in gold exploration. *J. Struct. Geol.* **26** 1087-1108.

WATERS PG, SMART PL and OSMASTON H (1990) Application of remote sensing to groundwater hydrology. *Remote Sens. Rev.* **4** 223-264.

WOOD ERIC F, SIVAPALAN M, BEVEN K and BAND L (1988) Effects of spatial variability and scale with implications to hydrologic modelling. *J. Hydrol.* **102** 29-47.

WOODFORD AC and CHEVALLIER L (2002) Regional Characterization and Mapping of Karoo Fractured Aquifer Systems – An Integration Approach using Geographical System and Digital Image Processing. WRC Report No. 653/1/02. Water Research Commission, Pretoria, South Africa. 40-55.

WOODS RA, SIVAPALAN M and DUNCAN M (1995) Investigating the representative elementary area concept: An approach based on field data. *Hydrol. Proc.* **9** (3/4) 291-312.

WU Y (2005) Groundwater Recharge Estimation in Table Mountain Group Aquifer Systems with a Case Study of Kammanassie Area. Ph.D. Thesis, University of the Western Cape (UWC). 108-122.

Available on website http://www.wrc.org.za
ISSN 0378-4738 (Print) = Water SA Vol. 36 No. 3 April 2010
ISSN 1816-7950 (On-line) = Water SA Vol. 36 No. 3 April 2010